Supplementary Information

Table S1. Existing methods for LiPON production.

Synthesis method	Source/precursors	Substrate needed?	Ionic conductivity (25℃)	Notes
Radio Frequency Sputtering[1]	Li_3PO_4	Yes	2.6×10^{-6} S/cm	
Pulsed Laser Deposition[2]	Li_3PO_4	Yes	1.6×10^{-6} S/cm	Rough surface
Atomic Layer Deposition[3]	lithium tert-butoxide, H_2O, trimethylphosphate	Yes	1.45×10^{-7} S/cm	Low growth rate
E-beam Evaporation[4]	Li_3PO_4	Yes	6.0×10^{-7} S/cm	
Ion Beam Sputtering[5]	Li_3PO_4	Yes	2.0×10^{-7} S/cm	Low growth rate
Metal-organic Chemical Vapor Deposition[6]	$Li(C_{11}H_{19}O_2)$, $(C_2H_5)_3PO_4$	Yes	2.95×10^{-7} S/cm	
Ammonolysis[7]	$Li_2O{\cdot}P_2O_5$ glass, NH_3	No	10^{-7}~10^{-9} S/cm	
Inductively Coupled Plasma[8]	Li_2O, $Li_4P_2O_7$, Li_4SiO_4, Si_3N_4	No	1.0×10^{-6} S/cm	Low LiPON purity, in nanopowder form
Ball Milling[9]	$LiPO_3$ and Li_3N	No	3.0×10^{-7} S/cm	Crystalline LiPON

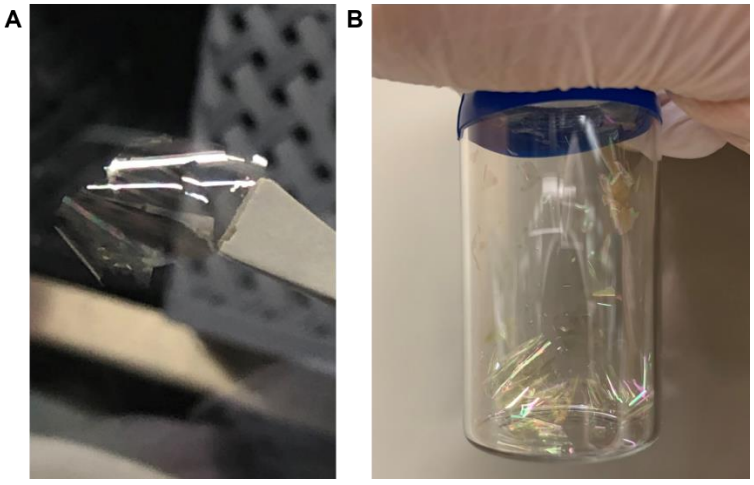

Figure S1. The photos of (A) a transparent and flexible FS- LiPON film and (B) FS-LiPON pieces in a capped battle.

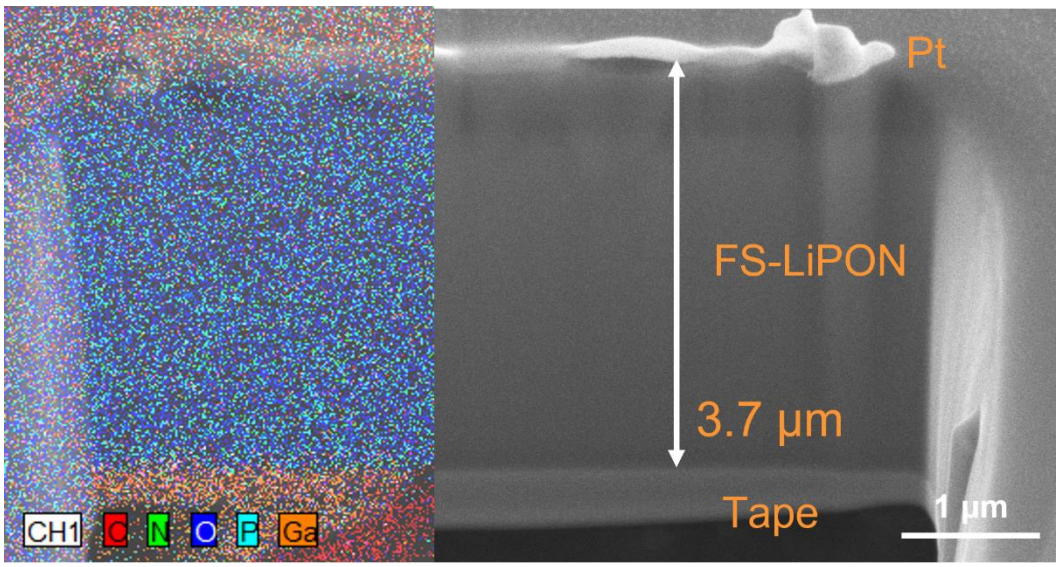

Figure S2. Cross-section image and EDS mapping of FS-LiPON.

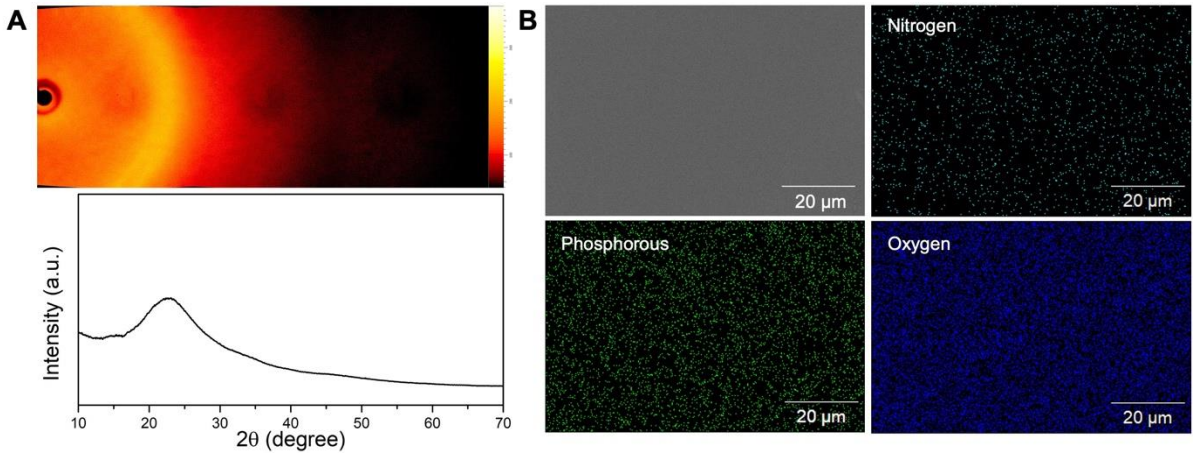

Figure S3. (A) XRD pattern of FS-LiPON thin film. (B) SEM image and EDS mapping on the surface of FS-LiPON.

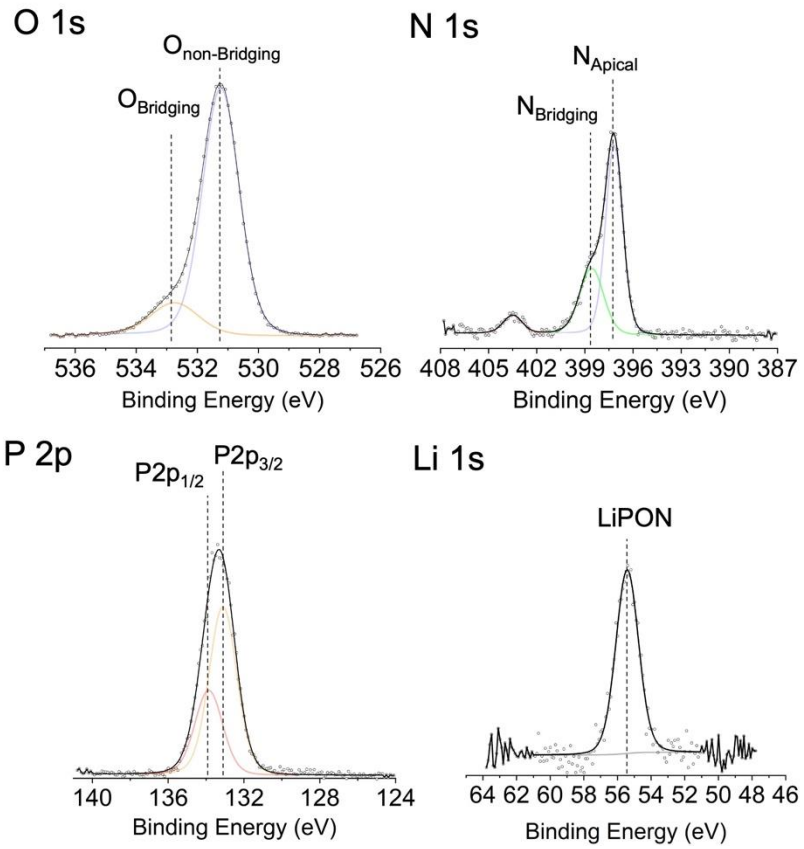

Figure S4. XPS spectra of O 1s, N 1s, P 2p and Li 1s regions of sub-LiPON thin film.

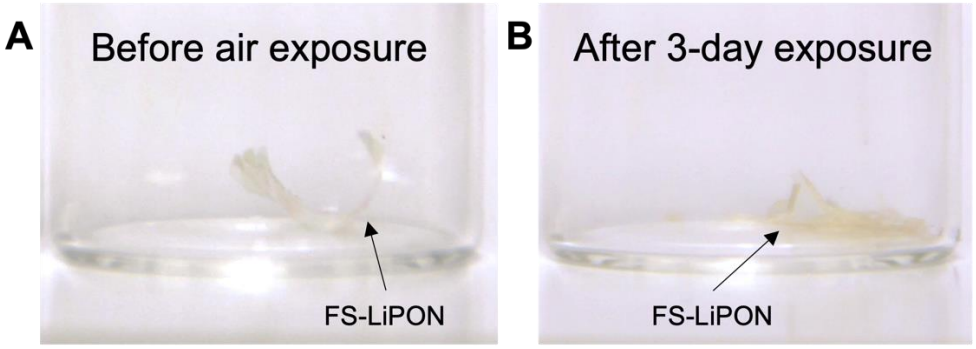

Figure S5. Photos of the same piece of FS-LiPON film before air exposure (A) and after air exposure (B), showing the film shape change due to stiffening.

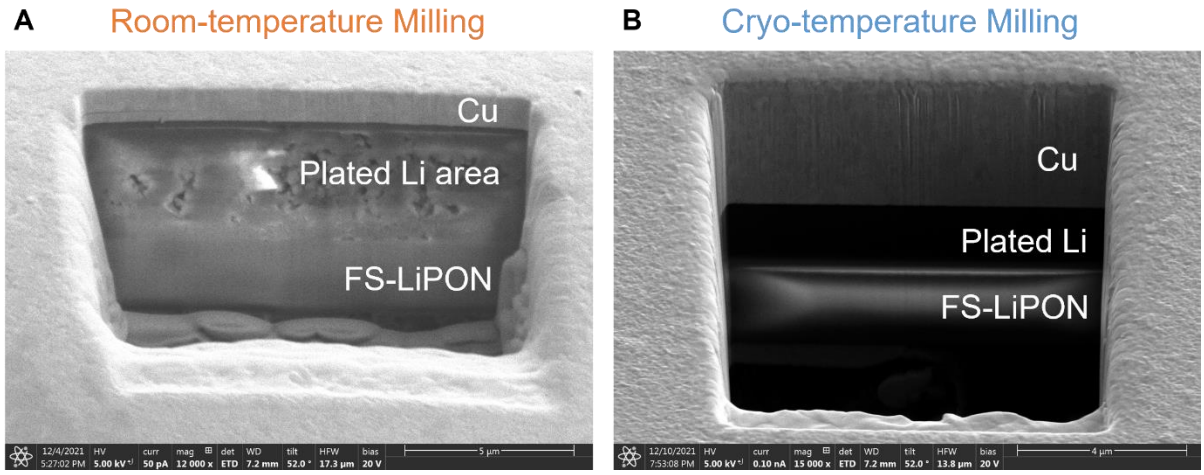

Figure S6. Cross-section FIB/SEM of the Li-Cu cell with ion milling performed at room temperature (A) and cryogenic temperature (-180°C). Morphology and contrast of plated Li metal in (A) have been changed due to the lack of cryogenic protection compared with (B).

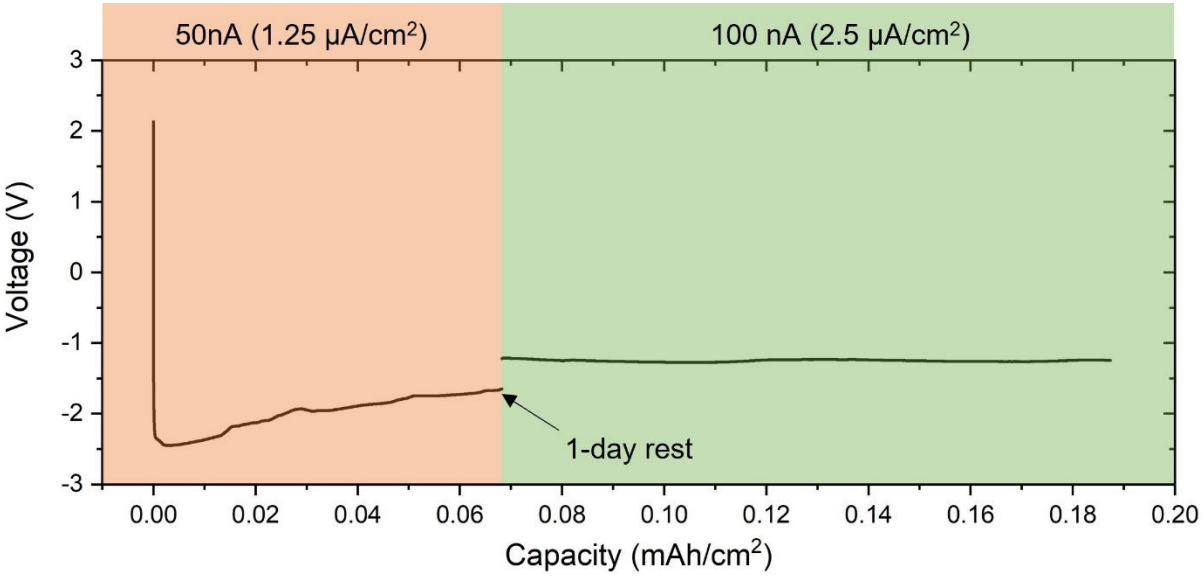

Figure S7. Voltage curve of Li metal plating with 1-day rest step.

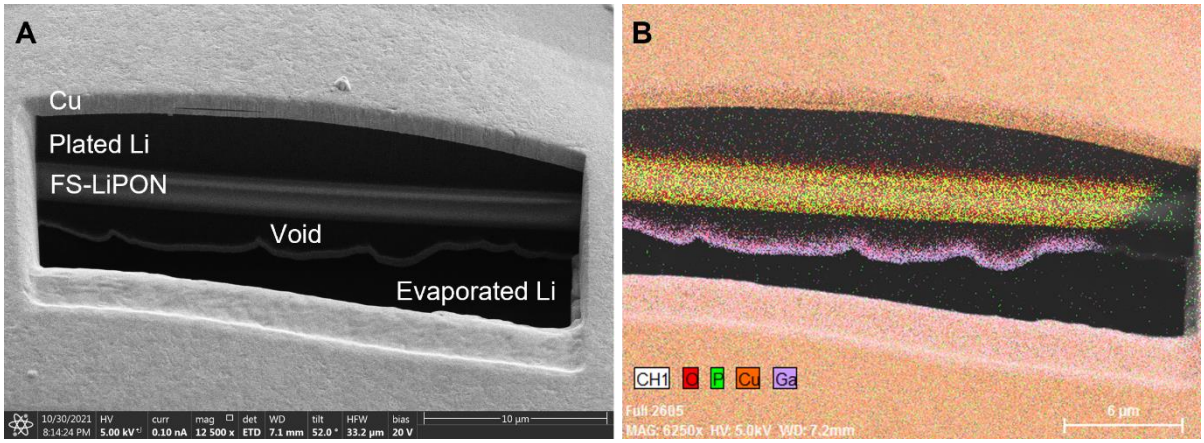

Figure S8. (A) Cross-section cryo-FIB/SEM image of the Li-Cu cell after plating. (B) EDS mapping of the corresponding area in (A).

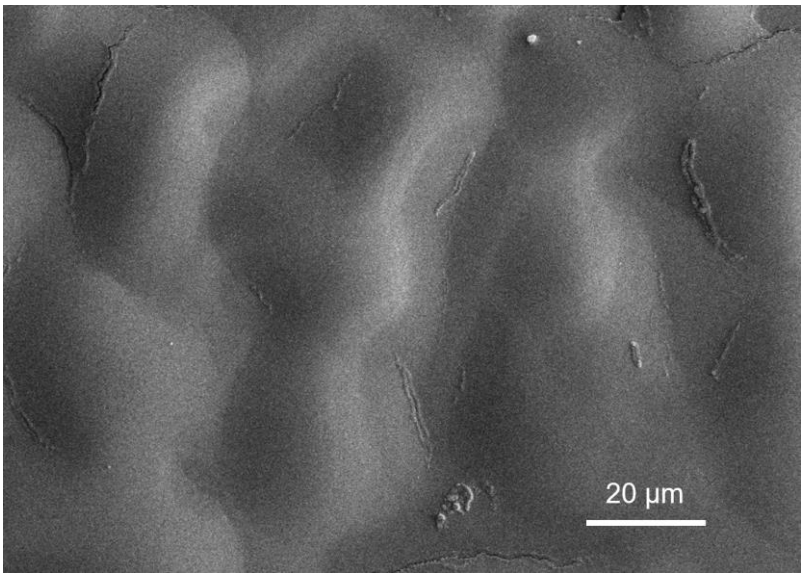

Figure S9. Top-view SEM image of Cu surface on the Li-Cu cell after Li metal plating.

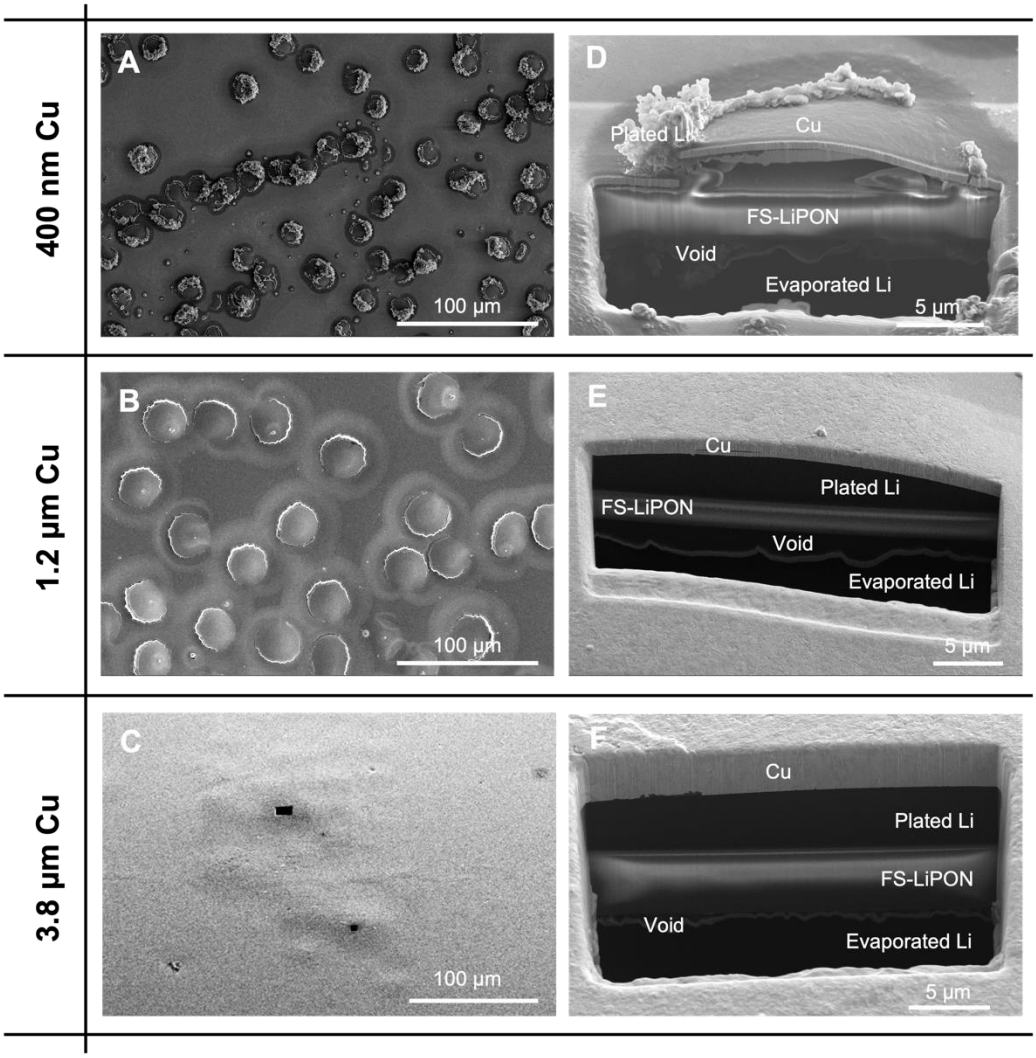

Figure S10. Top-view and cross-section SEM images of Li-Cu cell with different Cu thicknesses.

A

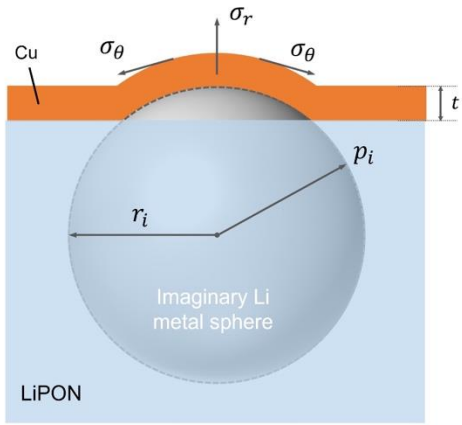

$$P = \frac{\varepsilon_{Cu} E_{Cu}}{(1-\nu_{Cu})} \cdot \left\{ \frac{3(r_i+t)^3}{2\left[(r_i+t)^3 - r_i^3\right]} - \frac{\nu_{Cu}}{1-\nu_{Cu}} \right\}^{-1}$$

ε_{Cu}: Strain in the circumferential directions
E_{Cu} :Young's modulus of Cu CC
t: Thickness of Cu CC
r_i: Radius of Cu CC imaginary sphere
κ: Curvature of Cu CC
ν_{Cu}: Poisson's ratio of Cu

B

	400 nm Cu	1.2 μm Cu	3.8 μm Cu
ε_{Cu}	0.052	0.030	0.024
E_{Cu} (GPa)	130	130	130
t (μm)	0.4	1.2	3.8
r_i	16.036	54.054	227.273
ν_{Cu}	0.34	0.34	0.34
σ (GPa)	**0.503**	**0.260**	**0.151**

Fi[1]gure S11. Stress analysis on Li-Cu cell with different Cu thicknesses. (A) Schematic of the model used for interfacial stress estimation and corresponding formula. (B) parameters and calculated stresses at Li/Cu interface with different Cu thicknesses.

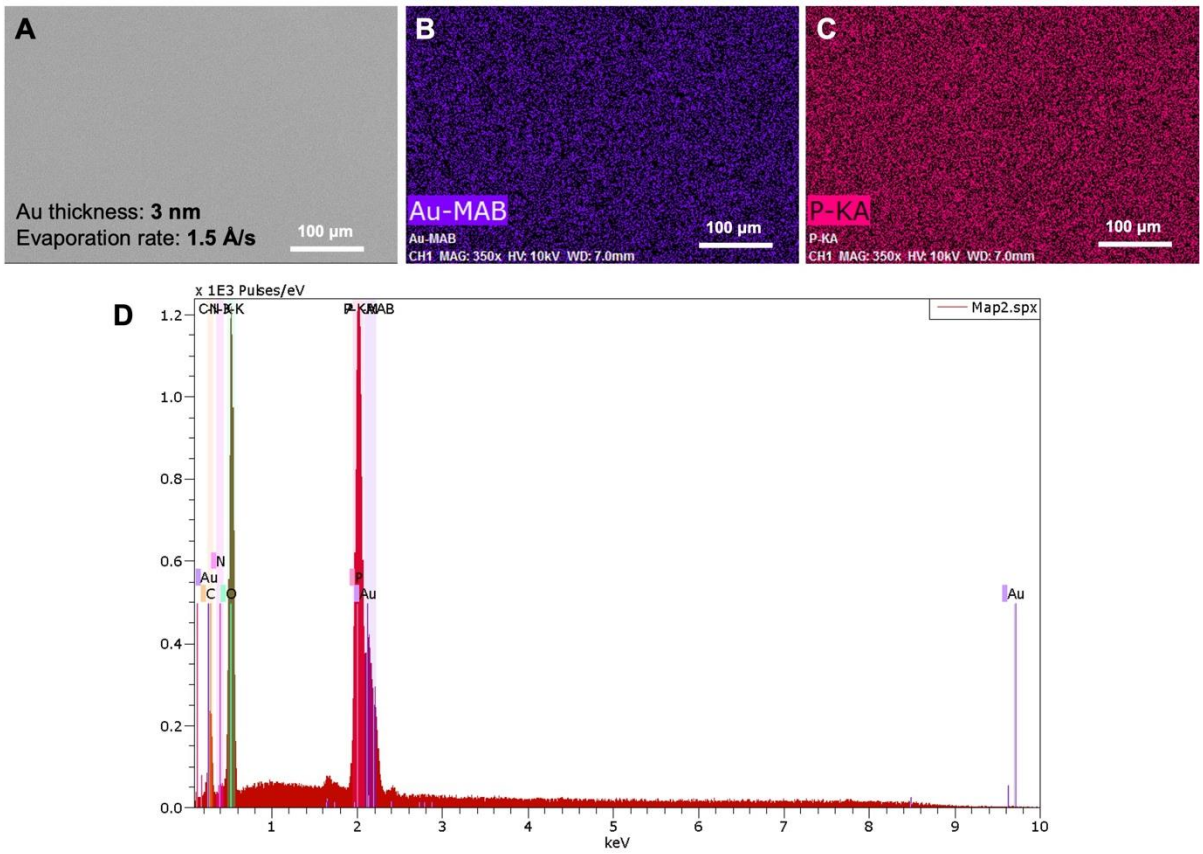

Figure S12. (A) Top-view SEM image of Au seeding layer on FS-LiPON. Au film thickness is 3 nm. EDS mapping results of Au signal (B) and P signal (C) in the same region, demonstrating the uniform evaporation of Au on FS-LIPON. (D) EDS spectrum collected from the region shown in (A).

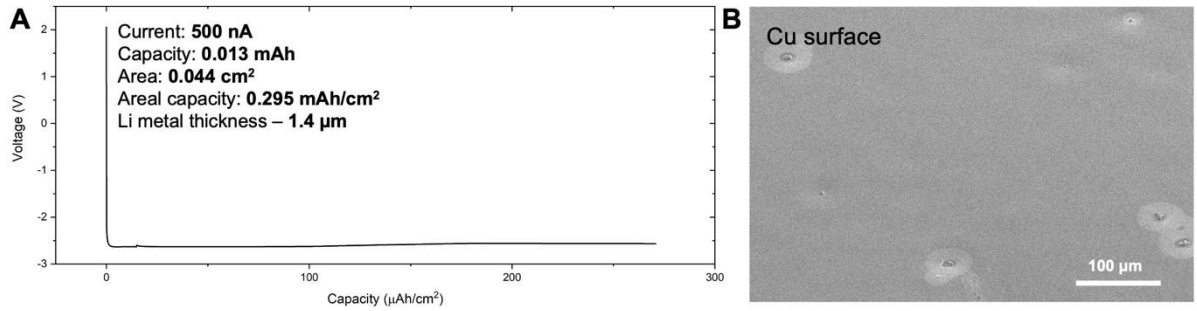

Figure S13. (A) Voltage curve of Li metal plating in Li-Cu cell with Au seeding layer. (B) Surface morphology of plated Li-Cu cell, showing a relatively smooth Cu surface and indicating uniform Li metal deposition.

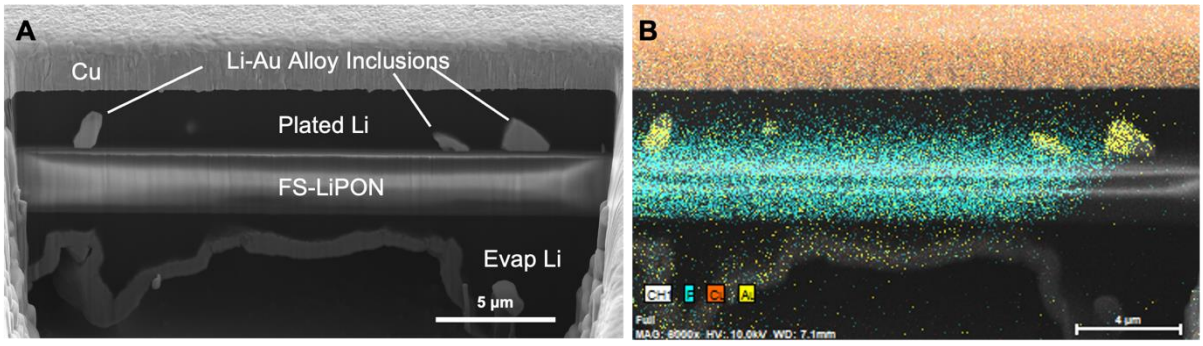

Figure S14. (A) Cross-section image of plated Li-Cu cell with Au seeding layer. Plated Li metal in this cell is ~3 µm in thickness. Inclusions within plated Li layer can be seen. (B) EDS mapping at the region shown in (A), suggesting the inclusions are Au-containing species.

References

1. Kozen, A. C., Pearse, A. J., Lin, C. F., Noked, M. & Rubloff, G. W. Atomic Layer Deposition of the Solid Electrolyte LiPON. *Chem. Mater.* **27**, 5324–5331 (2015).
2. J.B. Bates, N.J. Dudney, G.R. Gruzalski, R.A. Zuhr, A. Choudhury, C. F. L. Electrical properties of amorphous lithium electrolyte thin films. *Solid State Ionics* **29**, 42–44 (1992).
3. Zhao, S., Fu, Z. & Qin, Q. A solid-state electrolyte lithium phosphorus oxynitride film prepared by pulsed laser deposition. *Thin Solid Films* **415**, 108–113 (2002).
4. Liu, W. Y., Fu, Z. W., Li, C. L. & Qin, Q. Z. Lithium phosphorus oxynitride thin film fabricated by a nitrogen plasma-assisted deposition of E-beam reaction evaporation. *Electrochem. Solid-State Lett.* **7**, 36–41 (2004).
5. Nowak, S., Berkemeier, F. & Schmitz, G. Ultra-thin LiPON films - Fundamental properties and application in solid state thin film model batteries. *J. Power Sources* **275**, 144–150 (2015).
6. Kim, H. T., Mun, T., Park, C., Jin, S. W. & Park, H. Y. Characteristics of lithium phosphorous oxynitride thin films deposited by metal-organic chemical vapor deposition technique. *J. Power Sources* **244**, 641–645 (2013).
7. Muñoz, F., Durán, A., Pascual, L., Montagne, L., Revel, B. & Rodrigues, A. C. M. Increased electrical conductivity of LiPON glasses produced by ammonolysis. *Solid State Ionics* **179**, 574–579 (2008).
8. Westover, A. S., Kercher, A. K., Kornbluth, M., Naguib, M., Palmer, M. J., Cullen, D. A. & Dudney, N. J. Plasma Synthesis of Spherical Crystalline and Amorphous Electrolyte Nanopowders for Solid-State Batteries. *ACS Appl. Mater. Interfaces* **12**, 11570–11578 (2020).
9. López-Aranguren, P., Reynaud, M., Głuchowski, P., Bustinza, A., Galceran, M., López del Amo, J. M., Armand, M. & Casas-Cabanas, M. Crystalline LiPON as a Bulk-Type Solid Electrolyte. *ACS Energy Lett.* 445–450 (2021) doi:10.1021/acsenergylett.0c02336.